Differential and integral cross sections for the inelastic scattering of NO (X 2Π) by Ar based on a new ab initio potential energy surface

Millard H. Alexander

Citation: The Journal of Chemical Physics **99**, 7725 (1993); doi: 10.1063/1.465702
View online: http://dx.doi.org/10.1063/1.465702
View Table of Contents: http://scitation.aip.org/content/aip/journal/jcp/99/10?ver=pdfcov
Published by the AIP Publishing

Differential and integral cross sections for the inelastic scattering of NO ($X\ ^2\Pi$) by Ar based on a new *ab initio* potential energy surface

Millard H. Alexander
Department of Chemistry and Biochemistry, University of Maryland, College Park, Maryland 20742

(Received 9 June 1993; accepted 2 August 1993)

New *ab initio* potential energy surfaces for the Ar–NO ($X\ ^2\Pi$) system are reported based on correlated electron pair approximation (CEPA) calculations. The fitted, rigid-rotor surface was then used in full close-coupling calculations of differential and integral cross sections for excitation of NO at a center-of-mass energy of 442 cm^{-1} (0.0548 eV), as well as differential cross sections at lower energies of 119 and 149 cm^{-1} (0.0145 and 0.0185 eV). The calculated cross sections are compared with those determined using earlier electron-gas potential energy surfaces and with the results of available experimental measurements. In general, the new CEPA potential energy surfaces yield very good agreement with available experimental integral and differential cross sections. Both theory and experiment reveal a significant tendency for population of final rotational states of $\Pi(A'')$ reflection symmetry.

I. INTRODUCTION

Inelastic collisions involving closed-shell diatomic molecules in Π electronic states are considerably more complicated than those involving closed-shell molecules in $^1\Sigma$ electronic states. This is because the relative translational motion of the collision partners can couple not only with the rotational motion of the molecule, but also with the internal electronic (spin and/or electronic) angular momenta. Because the cylindrical degeneracy of a molecule in a Π electronic state is lifted by the approach of a collision partner, the description of the interaction of a Π state molecule with a closed-shell atom (or molecule) involves *two* electronic potential energy surfaces (PES).[1–6] The variation of the resulting inelastic cross sections with the final electronic-rotational state shows interesting propensities which are often reflective of interferences between collisions which sample to a greater or lesser extent one or the other of these PES's.[5,7,8]

Collisions of Ar atoms with NO in its electronic ground state have long served as the paradigm, both in experimental as well as theoretical studies, of inelastic collisions involving molecules in Π electronic states. Molecular beam studies have been reported of total differential cross sections[9,10] and of integral cross sections for inelastic scattering into individual final states.[11,12] Howard and co-workers[13,14] have carried out molecular-beam, electric-resonance spectroscopic investigations of the NO($X\ ^2\Pi$)Ar van der Waals molecule. Some years ago, Nielson, Parker, and Pack (NPP)[3] published approximate PES's for Ar–NO derived within the electron-gas model of Gordon and Kim.[15] There subsequently appeared[11,12,16–18] a number of scattering calculations based on the NPP PES's.

Within the past year, two groups have reported new molecular beam investigations[19–22] which yield *differential* state-resolved inelastic cross section for collisions of Ar with NO. The experiments by Gentry and co-workers[19,20] involved crossed molecular beams with subsequent angle-resolved laser-induced-fluorescence detection. These experiments were carried out at three values of the initial center-of-mass energy (119, 149, and 442 cm^{-1}). The highest energy was identical to that in the earlier *integral* cross section measurements of Joswig *et al.*[11,12] The experiments by Houston, Whitaker, and co-workers[21,22] involved a direct imaging technique for the measurement of the state-resolved differential cross sections at an even higher center-of-mass energy (1691 cm^{-1}).

Motivated by these two recent experiments, we have returned to the Ar–NO system. The present paper reports the determination of new *ab initio* PES's based on the use of the correlated electron pair approximation (CEPA) method[23–25] with a triple-zeta atomic orbital bases. The two relevant PES's, which correspond to the NO–Ar wave functions of A' and A'' reflection symmetry,[6] are then fitted and used in full close-coupled scattering calculations of the relevant differential and integral cross sections at a total energy of 442 cm^{-1}. These are then compared with similar calculations based on the earlier electron gas PES's of Nielson *et al.*[3] and with the results of experiment.[12,19,20]

II. *AB INITIO* CALCULATIONS

The $V_{A'}$ and $V_{A''}$ PES's were determined using the correlated electron pair (CEPA-1) method.[23–25] This method, which is size consistent and faster than multireference configuration interaction methods, has been used with considerable success to provide accurate potential energy surfaces for interactions of open-shell fragments with a noble gas target, in particular, NH–He,[26] OH–He,[27] and OH–Ar.[28] We used the recent augmented correlation-consistent valence triple-zeta (*avtz*) basis of Dunning and co-workers[29,30] (11*s*6*p*3*d*2*f* contracted to 5*s*4*p*3*d*2*f* for N and O and 16*s*10*p*3*d*2*f* contracted to 6*s*5*p*3*d*2*f* for Ar). Some exploratory calculations were carried out with the augmented correlation consistent quadruple zeta (*avqz-g*) basis[29,30] (13*s*7*p*4*d*3*f*2*g*) contracted to 6*s*5*p*4*d*3*f*2*g* for N and O and 17*s*12*p*4*d*3*f*2*g* contracted to 7*s*6*p*4*d*3*f*2*g* for Ar) and with the subset of this basis in which the *g* functions were not included (*avqz-f*). The *avtz*, *avqz-f*, and

TABLE I. The variation with the atomic orbital basis of the Ar–NO CEPA interaction energies (cm^{-1}) for colinear ($\theta=0°$; NO–Ar) approach of the Ar atom.[a]

R (bohr)	*avtz*	*avqz-f*	*avqz-g*
5.0	11 216.7	11 103.1	10 938.9
5.5	3 974.6	3 915.4	3 831.2
6.0	1 277.0	1 243.9	1 204.6
6.5	330.3	312.8	295.2
7.0	27.7	19.3	11.6
7.5	−50.8	−55.0	−57.7
8.0	−58.4	−61.0	−62.2
8.5	−47.9	−50.4	−50.7
9.0	−35.7	−37.3	−38.1
7.85[b]	−59.4		
7.81[b]		−62.6	
7.79[b]			−64.3

[a]See Sec. II for a discussion of the basis sets used.
[b]The last three rows indicate the position and depth of the minimum in the potential.

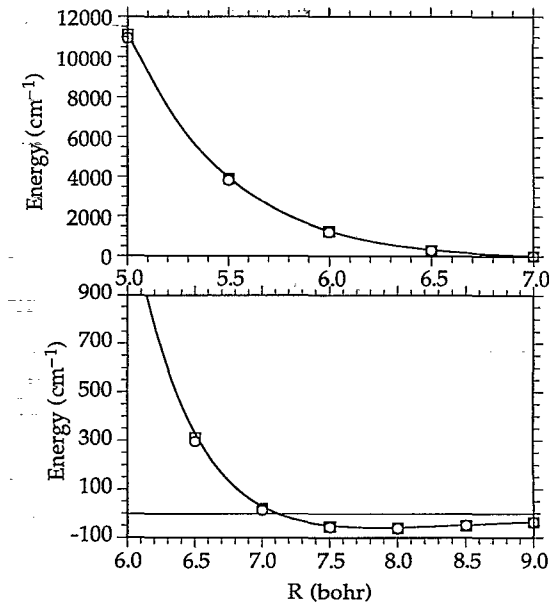

FIG. 1. A comparison of the CEPA-1 interaction potentials for collinear NOAr geometry determined using the *avtz* (solid curves), *avqz-f* (squares), and *avqz-g* (circles) atomic orbital bases. The lower panel is an enlargment of the comparison at long range.

avqz-g bases contained, respectively, a total of 142, 190, and 224 contracted Gaussian functions. In all the calculations reported here, the NO bond length was maintained at 2.1746 bohr, which corresponds to the experimental equilibrium internuclear distance in the NO molecule.[31] All calculations were carried out with the MOLPRO suite of *ab initio* programs.[32]

In C_s geometry, the two possible orientations of the NO 2π orbital correspond to a different point group (a' or a''). The interaction energy for each orientation can be defined as

$$V(R)=E_{\text{Ar–NO}}(R)-\Delta E_{\text{CP}}(R)-\Delta E_{\text{SC}}(R). \quad (1)$$

Here the counterpoise (CP) correction,[33] which adjusts for the lack of saturation of the orbital basis, is defined by[33]

$$\Delta E_{\text{CP}}=E_{\text{NO}}(R)+E_{\text{Ar}}(R)-E_{\text{NO}}(\infty)-E_{\text{Ar}}(\infty) \quad (2a)$$

and the residual size consistency (SC) of the calculations is defined by

$$\Delta E_{\text{SC}}=E_{\text{Ar–NO}}(\infty)-E_{\text{NO}}(\infty)-E_{\text{Ar}}(\infty). \quad (2b)$$

The geometry of the Ar–NO system will be described by the three Jacobi coordinates r (the NO bond length), R (the distance between the Ar atom and the center of mass of the NO molecules), and θ (the angle between **R** and **r**). As a calibration of the reliability of the *avtz* basis set, Table I and Fig. 1 compare the interaction energies for linear NO Ar geometry predicted by CEPA calculations with the *avtz*, *avqz-f*, and the *avqz-g* basis sets. The close agreement between the predictions of the *avtz* and the *avqz-f* bases indicates that the former, smaller basis is sufficiently complete with respect to including additional *s, p, d,* or *f* functions. It is also apparent that the addition of *g* functions has only a small effect, leading to a slight contraction of the repulsive wall and a slight increase in the attractive tail of the potential.

As a calibration of the accuracy of the CEPA method, we have performed complete-active-space self-consistent field (CASSCF) calculations followed by multireference configuration interaction (MRCI) calculations for the approach of the Ar atom at a Jacobi angle of $\theta=90°$. In these calculations, done with the same *avtz* atomic orbital basis used in the CEPA calculations, the active space in the CASSCF calculations was constructed by distributing the seven electrons among the four outermost valence orbitals of NO (5σ, 1π, 2π, and 6σ).

In the subsequent, internally contracted,[34,35] configuration interaction (CI) calculations, the reference space was generated by including all (six) configurations with weights greater than 0.04 in the CASSCF wave function. The CI calculations included all single and double excitations out of this reference space with the exclusion of excitations out of the lowest six orbitals of a', and the lowest two orbitals of a'', symmetry (which correspond to the $1s$ orbitals of each atom and the $n=2$ shell of Ar). The total number of contracted (uncontracted) configurations used was 866 623 (12 730 252) and 873 498 (12 618 489) for the states of A' and A'' symmetries, respectively. The contribution of higher-order excitations was then estimated using the multireference version of the averaged coupled-pair functional (ACPF) method of Gadnitz and Ahlrichs.[36] A few additional calculations were done by including in the reference space all (nine) configurations with weights greater than 0.02 in the CASSCF wave function. This increase in the reference space had a negligible effect on the calculated interaction energies.

Table II and Fig. 2 compare values of the CEPA, MRCI, and MRACPF interactions energies for the perpendicular approach of the Ar atom ($\theta=90°$). The self-consistency corrections are large, especially for the MRCI calculations. Notwithstanding, the CEPA and MRACPF calculations agree extremely well. The MRCI calculations

TABLE II. Ar–NO interaction energies (cm^{-1}) for perpendicular ($\theta=90°$) approach of the Ar atom.[a]

R (bohr)	V_{CEPA}	V_{MRCI}	V_{MRACPF}	ΔE_{CP}[b]
A' potential				
5	2060.5	2291.3	2115.7	157.5
6	97.0	185.9	105.0	70.8
7	−76.9	−38.3	−78.9	31.1
8	−50.9	−31.8	−54.4	17.4
9	−26.3	−15.0	−29.7	9.7
A'' potential				
5	1989.6	2276.2	2089.4	144.6
6	86.5	195.2	114.2	66.3
7	−76.0	−35.3	−74.4	29.5
8	−50.3	−33.6	−54.8	16.5
9	−26.4	−14.8	−28.8	9.3
ΔE_{SC}[c]	0.0	6536.7	−2214.6	

[a]In these calculations, the NO bond distance was held at $r=2.1746$ bohr, the experimental equilibrium bond length (Ref. 31).
[b]This counterpoise correction is defined by Eq. (2a) of the text. The values listed are the counterpoise corrections for the CEPA calculations. The MRCI and MRACPF values were virtually identical to those tabulated.
[c]The size-consistency correction is defined by Eq. (2b) of the text.

underestimate, by about 40%, the depth of the attractive well. Unfortunately, the MRACPF calculations require considerably more computer time, so that it was not feasible to determine the complete PES's with this method.

CEPA calculations of the A' and A'' Ar–NO potential energy surfaces were carried out at 11 values of θ ($\theta=0°$, 20°, 40°, 60°, 80°, 90°, 100°, 120°, 140°, 160°, and 180°) and nine values of the center-of-mass separation R (5.5, 6, 6.5, 7, 7.5, 8, 8.5, 9, and 10 bohr). The NO bond distance was held to $r=2.1746$ bohr, the experimental equilibrium bond length.[31] Additional calculations at $\theta=90°$ were carried out for $R=5$ bohr.

For each value of θ, the $V_{A'}$ and $V_{A''}$ PES's were fit as a function of R to the general functional form[37]

$$V(R,\theta_i)=c_1\exp(-b_1R)+(c_2+c_3R)\exp(-b_2R)+c_4\{\tanh[1.2(R-R_0)]-1\}/R^6. \quad (3)$$

The rms relative error in the fit was $<0.1\%$.

In the subsequent scattering calculations, it is more convenient to use the average and the difference of the $V_{A'}$ and $V_{A''}$ PES's which we define as[6]

$$V_{sum}(R,\theta)=0.5[V_{A''}(R,\theta)+V_{A'}(R,\theta)] \quad (4a)$$

and

$$V_{dif}(R,\theta)=0.5[V_{A''}(R,\theta)-V_{A'}(R,\theta)]. \quad (4b)$$

The angular dependence of these two PES's is expanded as[6]

$$V_{sum}(R,\theta)=\sum_{\lambda=0}^{\lambda_{max}} V_{\lambda 0}(R)d^{\lambda}_{00}(\theta) \quad (5a)$$

and

$$V_{dif}(R,\theta)=\sum_{\lambda=2}^{\lambda_{max}} V_{\lambda 2}(R)d^{\lambda}_{20}(\theta), \quad (5b)$$

where $d^{\lambda}_{mn}(\theta)$ is a reduced rotation matrix element.[38] Because $d^{\lambda}_{00}(\theta)$ is equal to the regular Legendre polynomial

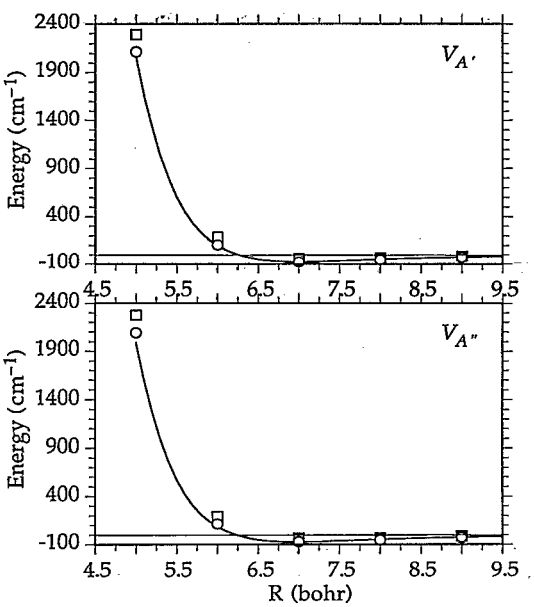

FIG. 2. A comparison of the CEPA-1 (solid curves), MRCI (squares), and MRACPF (circles) $V_{A'}$ (upper panel) and $V_{A''}$ (lower panel) Ar–NO PES's for the perpendicular ($\theta=90°$) approach of the Ar atom.

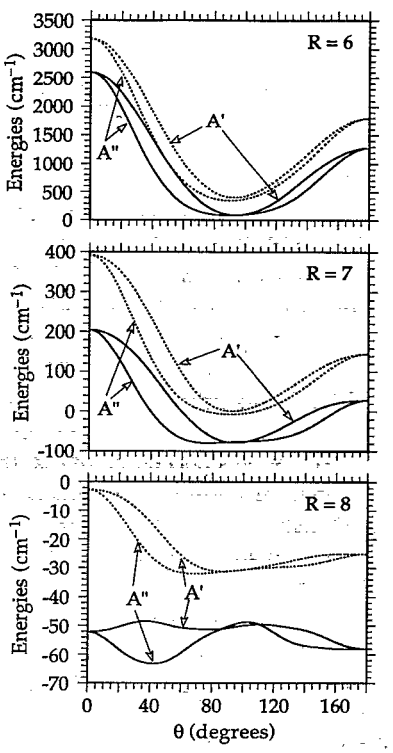

FIG. 3. Plots of the dependence on the Ar–NO angle (with $\theta=0$ corresponding to collinear ArNO) of the $V_{A'}$ and $V_{A''}$ PES's for three values of the center-of-mass separation (in bohrs). The predictions of the *ab initio* calculations reported here are indicated by solid curves, while the predictions of the earlier electron-gas calculations of Ref. 3 are indicated by dashed curves.

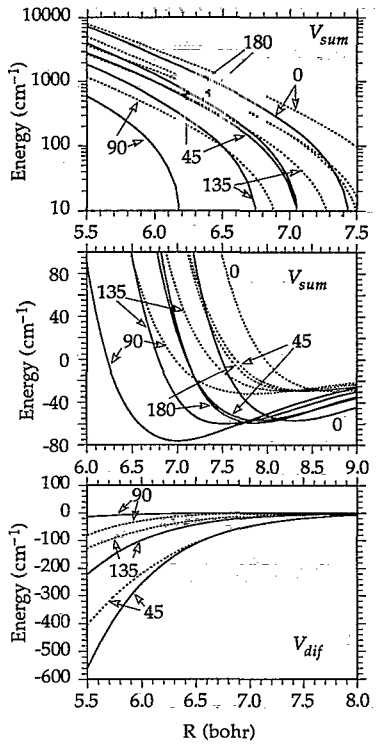

FIG. 4. Plots of the dependence on the Ar–NO center-of-mass separation of the *sum* and *difference* PES's [Eq. (7)] for five values of the angle (with $\theta=0$ corresponding to collinear ArNO). The predictions of the *ab initio* calculations reported here are indicated by solid curves, while the predictions of the earlier electron-gas calculations of Ref. 3 are indicated by dashed curves.

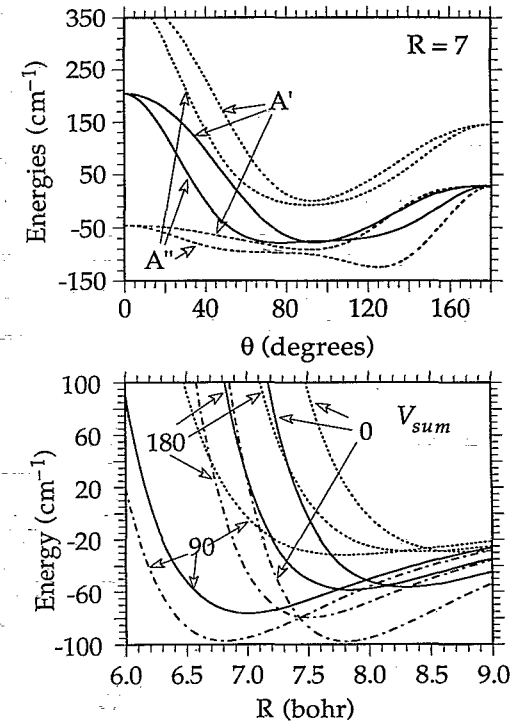

FIG. 5. (Upper panel) The plot of the dependence on the Ar–NO angle (with $\theta=0$ corresponding to collinear ArNO) of the $V_{A'}$ and $V_{A''}$ PES's for an Ar–NO center-of-mass separation of 7.0 bohr. (Lower panel) The plot of the dependence on the Ar–NO center-of-mass separation of the *sum* PES's [Eq. (7)] for collinear and perpendicular approaches (with $\theta=0$ corresponding to collinear ArNO). In both panels, the predictions of the *ab initio* calculations reported here are indicated by solid curves, while the predictions of the earlier electron-gas calculations of Ref. 3 are indicated by dashed curves and the predictions of the modified NPP potential as defined in Ref. 12 are indicated by dotted–dashed curves.

$P_\lambda(\cos\theta)$,[38] Eq. (5a) is identical to the more often seen Legendre expansion. Here we took λ_{max} equal to 10, the upper limit imposed by the number of different values of θ at which *ab initio* calculations were carried out.

Figure 3 compares the dependence on θ of the $V_{A'}$ and $V_{A''}$ CEPA PES's with the earlier electron-gas PES of NPP,[3] computed from the analytical expression given by these authors, for three values of the Ar–NO distance. A similar comparison is the subject of Fig. 4, but as a function of the center-of-mass separation R at five fixed values of the angle θ. The PES surfaces are qualitatively similar and predict, in both cases, a less repulsive interaction when the lone NO 2π electron lies perpendicular to the triatomic plane (the A'' PES). In addition, both CEPA PES's are uniformly less repulsive than the corresponding electron-gas PES's for the following reason: As the Ar atom approaches the NO molecule, the electron distribution of both species can reorganize somewhat to lower the interaction energy. This effect is contained in any *ab initio* treatment, but not in an electron-gas treatment, in which no relaxation of the charge distribution of the isolated partners is permitted.

To compensate for this rigidity, Nielson, Parker, and Pack suggested several modifications in the parameters which described the fit to their *ab initio* points.[3] In subsequent scattering calculations Joswig, Andresen, and Schinke (JAS)[12] incorporated these modifications to the *sum* PES, while leaving the *difference* PES unchanged. Figure 5 compares the predictions of this modified NPP PES with the original NPP PES and with our CEPA potential. We observe that the modifications introduced by Joswig and co-workers[12] results in a V_{sum} which is now less repulsive than the *ab initio* potential and which possesses a deeper well.

Figure 6 displays contour plots of the A' and A'' PES in the region of the minima in the CEPA surfaces. The minimum on the A'' PES ($R=7.1$ bohr, $\theta=73°$, $D_e=79.1$ cm^{-1}) lies only slightly (1.3 cm^{-1}) lower in energy than the minimum on the A' surface ($R=7.0$ bohr, $\theta=94°$), but is much broader. By way of comparison, the earlier electron-gas surface of NPP (Ref. 3) predicts a slighter deeper minimum on the A'' surface at $R=7.43$ bohr and $\theta=89.3°$. The modified NPP potential used by JAS[12] also predicts the lower minimum to occur on the A'' PES, but the geometry of the minimum ($R=7.0$ bohr, $\theta=124.4°$) is considerably different than that predicted by our *ab initio* calculations and the well is considerably deeper ($D_e=124.7$ cm^{-1}).

Both the spectroscopic[13] and molecular beam, total differential cross section experiments[9,10] predict the minimum in the Ar–NO potential to occur for T-shaped geometries

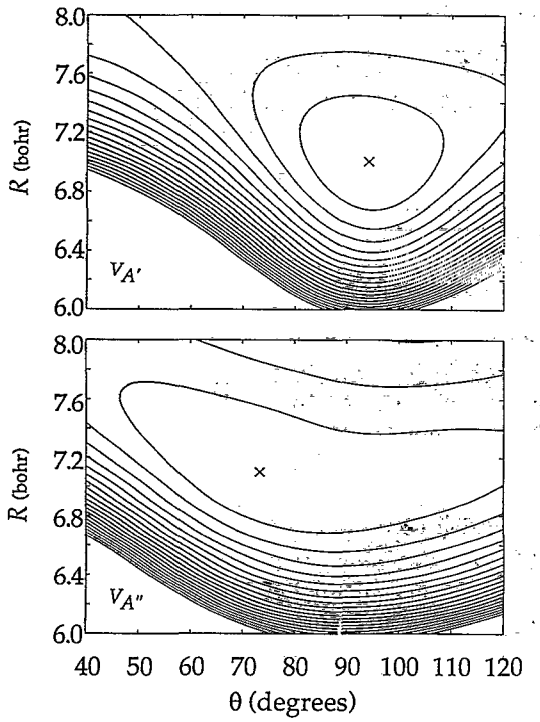

FIG. 6. Contour plots of the Ar–NO $V_{A'}$ and $V_{A''}$ PES's in the region of the minima in these surfaces. The zero of energy is taken to be the minimum on the A'' potential, which occurs at an energy of -79.1 cm^{-1} with respect to the separated species. In both panels, the contours are equally spaced at 10 cm^{-1} intervals, with the first contour at 10 cm^{-1} and the final contour at 200 cm^{-1} with respect to this energy origin. The positions of the minima are indicated by x's. The minimum on the A' potential lies 1.3 cm^{-1} above the minimum on the A'' potential.

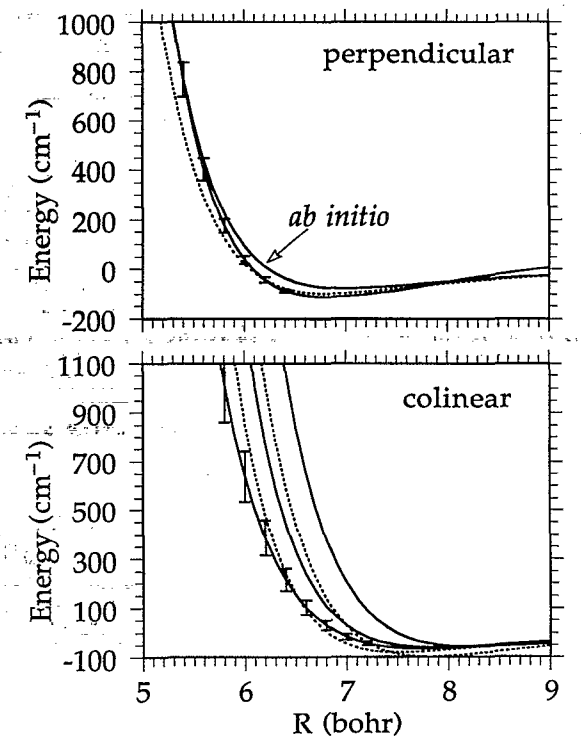

FIG. 7. A comparison of the sum potential energy surface for Ar–NO [Eq. (7)] as predicted by the present *ab initio* calculations and from the deconvolution of the total differential cross section scattering experiments of Casavecchia *et al.* (Ref. 10). The upper panel compares the PES's for perpendicular geometry, while the lower panel compares the PES's for collinear geometry. The indicated error bars reflect the uncertainty arising from the error bars in the experimental anisotropy parameters A_2 and B_2 (Ref. 10). Finally, the dashed curves indicate the predictions of the modified NPP potential (Refs. 3 and 12).

at center-of-mass separations of, respectively, 7.01 (Ref. 13), 7.29 (Ref. 9), and 7.10 bohr (Ref. 10) (3.711, 3.86, and 3.77 Å), which agree well with the results of the present calculations. The spectroscopic studies[13] were found to be consistent with an assignment of A'' reflection symmetry to the electronic wave function of the Ar···NO van der Waals molecule and found that the vibrationally averaged position of the Ar atom was tipped out of a pure T-shaped geometry $\sim 5°$ towards the N end. Our *ab initio* results are consistent with both these conclusions.

In the interpretation of the total differential cross section experiments, the electronic asymmetry of NO was ignored, which is equivalent to the assumption that the $V_{\rm dif}$ PES is vanishingly small. An additional approximation restricted the expansion of the $V_{\rm sum}$ PES to only the $\lambda=0$ and 2 terms [Eq. (5a)]. Figure 7 compares, for $\theta=0°$, 90°, and 180°, the dependence on the Ar–NO separation of our *ab initio* sum potential with the experimentally derived potential of Casavecchia *et al.*[10] and with the modified NPP sum potential of JAS.[12] The agreement is excellent for the perpendicular approach of the Ar atom to the NO molecule. However, the experimental PES is seen to be considerably less repulsive for the collinear approach.

The differences between the experimental and CEPA potentials for the collinear approach are much larger than what we would anticipate to be the residual errors in the calculated potential energy surface. Figures 1 and 2 strongly suggest that an eventually more complete treatment of electron correlation would render the calculated potentials only slightly less repulsive. An additional shortcoming in the PES derived from the total differential cross section measurements[10] is the lack of any *odd-*λ terms in the Legendre expansion (8) of the potential. Thus, the derived $V_{\rm sum}$ PES cannot describe the considerable difference in the degree of repulsivity for the approach of the Ar atom to the two ends of the NO molecule, which is clearly apparent in the CEPA PES as shown in Fig. 7.

III. FORMAL ANALYSIS OF $^2\Pi$ SCATTERING

The total Hamiltonian for the collision of a diatomic molecule with a structureless atom can be written as

$$H(r,R,\theta,q)=-\frac{\hbar^2}{2\mu R^2}\frac{\partial}{\partial R}R^2\frac{\partial}{\partial R}+\frac{\mathbf{l}^2}{2\mu R^2}+H_{\rm mol}(r,q)+V(r,R,\theta,q). \quad (6)$$

Here q designates, collectively, the electronic coordinates, μ denotes the collision reduced mass of the atom + diatomic system, and $\mathbf{l}$ designates the operator for the orbital angular momentum of the molecule with respect to the atom.

The internal Hamiltonian for the diatomic molecule $H_{\rm mol}(r,q)$ in Eq. (1) can be written as

$$H_{\rm mol}(r,q)=-\frac{\hbar^2}{2mr^2}\frac{\partial}{\partial r}r^2\frac{\partial}{\partial r}+\frac{(\mathbf{J}-\mathbf{L}-\mathbf{S})^2}{2mr^2}+H_{\rm so}(q;r)$$
$$+H_{\rm el}(q;r). \quad (7)$$

Here m is the reduced mass of the diatomic, **J**, **L**, and **S** designate, respectively, the total, electronic orbital, and spin angular momentum of the molecule ($S=1/2$ and $L=1$ for a $^2\Pi$ molecule); $H_{\rm so}(q;r)$ is the spin–orbit operator; and $H_{\rm el}(q;r)$ is the usual Born–Oppenheimer electronic Hamiltonian.

In the quantum close-coupled treatment of the scattering, it is most convenient to expand the total wave function as a sum of products of wave functions which are eigenfunctions of the molecular Hamiltonian, multiplied by functions which describe the orbital motion of the noble gas collision partner with respect to the diatomic molecule. The electronic-rotational wave functions of the NO molecule can be expressed most generally in an intermediate coupling basis as[39,40]

$$|JMF_1\epsilon\rangle=\cos\chi_J|JM,\Omega=\tfrac{1}{2},\epsilon\rangle+\sin\chi_J|JM,\Omega=\tfrac{3}{2},\epsilon\rangle \quad (8)$$

and

$$|JMF_2\epsilon\rangle=-\sin\chi_J|JM,\Omega=\tfrac{1}{2},\epsilon\rangle+\cos\chi_J|JM,\Omega=\tfrac{3}{2},\epsilon\rangle, \quad (9)$$

where the pure Hund's case (a) wave functions are denoted by $|JM\Omega\epsilon\rangle$ with parity index $\epsilon=+1$ and $\epsilon=-1$ for, respectively, the e and f labeled Λ-doublet states.[41] Here M and Ω designate the space- and molecule-frame projections of **J**. The F_1 and F_2 labels designate the lower and higher (in energy) of the two spin–orbit manifolds.

The mixing angle χ_J in Eqs. (8) and (9) is obtained by diagonalization of the 2×2 molecular Hamiltonian which represents the coupling between the Hund's case (a) wave functions due to the spin–rotation ($\mathbf{J}\cdot\mathbf{S}$) term which arises in the expansion of the $(\mathbf{J}-\mathbf{L}-\mathbf{S})^2/2\mu r^2$ term in Eq. (1).[42,43] For NO at low J, in the pure case (a) limit, χ_J approaches 0. As J increases and the rotational spacing becomes large compared to the spin–orbit splitting, the Hund's case (b) limit is approached and χ_J approaches $\pi/2$. For NO, where the rotational constant B is small [1.672 $\rm cm^{-1}$ (Ref. 31)] with respect to $A_{\rm so}$ [119.8 $\rm cm^{-1}$ (Ref. 31)], this mixing starts to become significant for $J>10.5$.[44] In the case (b) limit, where $BJ\gg|A_{\rm so}|$, the F_1 and F_2 wave functions become an equal admixture of the $\Omega=1/2$ and $\Omega=3/2$ case (a) basis functions.

To describe the collision, one expands the wave function of the composite system consisting of the molecule and scattering partner in terms of products of molecular eigenfunctions and wave functions describing the relative orbital motion of the collision system.[5,45,46] This corresponds to the asymptotically correct description of the atom +diatom system. Scattering amplitudes and cross sections for transitions between individual $|JMF_i\epsilon\rangle$ multiplet levels can then evaluated by solution of the close coupled (CC) equations.[5,45,46] To solve these equations, one must first evaluate matrix elements of the interaction potential $V(r,R,\theta,q)$ in the intermediate coupling basis. For brevity, we shall not reproduce these lengthy expressions here, but refer the interested reader to our earlier article.[8] Integral and differential cross sections can be obtained in the usual manner from the asymptotic form of the solution to these CC equations.[5] Implicit in the present, as well as all earlier, treatments of collisions involving molecules in $^2\Pi$ electronic states[11,12,16–18,47] is the assumption that the matrix elements of the terms $H_{\rm so}(q;r)$ and $(\mathbf{J}-\mathbf{L}-\mathbf{S})^2/2mr^2$ in the molecular Hamiltonian [Eq. (7)] are *unchanged* from their values in the isolated diatomic.

In the case (a) limit, where Ω is a good quantum number, transitions between levels in the *same* spin–orbit manifold ($\Omega'=\Omega$) will be coupled only by the $V_{\lambda0}(R,r)$ terms in the expansion of the potential [Eq. (5a)], while transitions between levels in *different* spin–orbit manifolds ($\Omega'\neq\Omega$) will be coupled only by the $V_{\lambda2}(R,r)$ terms in the expansion of the potential [Eq. (5b)].[5,6] In other words, inelastic transitions within a given spin–orbit manifold will be governed by the *average* of the $V_{A'}$ and $V_{A''}$ potential energy surfaces, while inelastic transitions from one spin–orbit manifold to the other will be governed by the *difference* between the $V_{A'}$ and $V_{A''}$ potentials.

Furthermore, in the case (a) limit, all matrix elements of the potential between states labeled by quantum numbers $JF_i\epsilon$ and $J'F_i'\epsilon'$ contain the phase factor $1-\epsilon\epsilon'(-1)^{J+J'+l}$ [see Eq. (29) of Ref. 6]. Thus the *odd-λ* terms in the expansion of both the sum and difference PES's will couple ϵ-conserving (e/f conserving) transitions with *odd* ΔJ and ϵ-changing (e/f changing) transitions with *even* ΔJ. The reverse will hold for the *even-λ* terms in the expansion of the PES's.

In intermediate coupling, the mixing of the case (a) basis states [Eqs. (8) and (9)] implies that transitions involving any pair of $|JMF_i\epsilon\rangle$ multiplet levels will be coupled by *both* the $V_{\lambda0}(R)$ and $V_{\lambda2}(R)$ terms in the expansion of the potential. These terms will add constructively or destructively depending on the initial and final multiplet labels.[8] The magnitude of the resulting cross sections will be sensitive to this quantum interference, so that the simple case (a) propensity rules[5] will no longer be valid. As we have shown,[8] depending on the sign of the difference between $V_{A'}$ and $V_{A''}$, one can in some cases predict a propensity for selective populations of final states which are either *symmetric* (A'; F_1e or F_2f) or *antisymmetric* (A''; F_1f or F_2e) with respect to reflection of the spatial part of the electronic wave function in the plane of rotation of the $^2\Pi$ molecule.[8,40,48]

A particular example of this quantum interference will occur when an initial, low-J state is well described in Hund's case (a), but the final state, at considerably higher J, is better described in intermediate case coupling. Because the wave function of the final state represents a linear combination of case (a) wave functions,[49] the probabilities for transitions from a low-J to high-J level will involve quantum interference between scattering on the $V_{A'}$ and $V_{A''}$ PES's. Consequently, the cross sections for transitions

out of a low-J level into levels of high J, even averaged over both initial Λ-doublet levels, may favor final states of a particular reflection symmetry.

In our earlier, formal investigation of collisions of NO with a flat surface,[49] we have used the energy sudden limit[50,51] to predict this effect. This was confirmed by subsequent calculations.[44,52] In general, a transition from the initial rotational level J to final level J' will be directly coupled by the potential only when $\Delta J \equiv |J-J'|$ is less than (or equal to) the largest value of the index λ which appears in the expansion of the potential energy surfaces in terms of reduced rotation matrix elements [Eq. (5)]. In the present case, $\max(\lambda)=10$, so that transitions into the final states of NO where a sizable mixing of the $\Omega=1/2$ and $\Omega=3/2$ wave functions occurs ($J>10.5$) will not be directly coupled by the potential. Thus one cannot make a prediction of the relative strength of the transitions into levels of A' or A'' symmetry merely from examination of the size of the coupling matrix elements.

In the subsequent investigation of this propensity, it will be useful to define *definite-symmetry* cross sections (either integral or differential) which, for a given $JF_1 \rightarrow J'F_i$ transition, are the *sum* of the two fully resolved, but degeneracy-averaged, cross sections which lead to population of the J' Λ-doublet levels of either $\Pi(A')$ or $\Pi(A'')$ reflection symmetry. For transitions into the F_1 manifold, these definite symmetry cross sections can be written as

$$\sigma(JF_1 \rightarrow J'F_1;A') = \sigma(JF_1 e \rightarrow J'F_1 e) + \sigma(JF_1 f \rightarrow J'F_1 e), \quad (10a)$$

$$\sigma(JF_1 \rightarrow J'F_1;A'') = \sigma(JF_1 e \rightarrow J'F_1 f) + \sigma(JF_1 f \rightarrow J'F_1 f). \quad (10b)$$

The two right-hand sides will be interchanged for $F_1 \rightarrow F_2$ transitions, since in the latter case, it is the f levels which are associated with $\Pi(A')$ reflection symmetry.[48]

In the molecular beam experiments,[12,19–22] the initial state Λ-doublet levels of the NO molecule are not selected and are assumed to be equally populated. In addition, in most cases, the final Λ-doublet levels of the scattered molecule were not resolved. In this case, the appropriate comparison with experiment involves Λ-doublet averaged, rotationally inelastic cross sections, which we define as the *average* of the cross sections defined above, namely,

$$\sigma(JF_i \rightarrow J'F_i') = 0.5[\sigma(JF_i \rightarrow J'F_i;A') + \sigma(JF_i \rightarrow J'F_i;A'')]. \quad (11)$$

IV. DETERMINATION OF CROSS SECTIONS

Both the *ab initio* potential energy surfaces described in Sec. II as well as the earlier electron-gas potential of Nielson *et al.*[3] were used in the present scattering calculations. These were carried out with our HIBRIDON package,[46] within the exact coupled channel (CC) formulation without any dynamical approximations, at total energies of 117, 149, and 442 cm^{-1}. The integration parameters were all adjusted to ensure convergence of the calculated S matrix elements to an accuracy of better than 1:10.[4] The maximum value of the total angular momentum (the partial wave index) used in the calculations was taken to be, at the three respective energies, 75.5, 85.5, and 135.5, which ensured convergence of both the calculated integral cross sections as well as the calculated differential cross sections over the range of angles sampled in the experiments of Jons *et al.*[19,20] The maximum NO rotational quantum number included in the channel basis was, again for the three respective energies, 13.5, 14.5, and 16.5, which ensured that all the energetically open levels, and at least one closed level, were included. In the calculations at 442 cm^{-1}, the total number of channels in the resulting CC calculations was 610.

V. INTEGRAL INELASTIC CROSS SECTIONS

Figure 8 presents the Λ-doublet averaged integral cross sections for transitions out of the $J=0.5$ F_1 level into higher levels of both the F_1 and F_2 spin–orbit manifolds of NO at an initial collision energy of 442 cm^{-1}. In the upper panel, the cross sections calculated from the CEPA potential for transitions into rotational levels of the F_1 spin–orbit manifold are compared with the experimental data of JAS.[12] The latter are normalized by multiplication by a factor of 0.534, chosen so that the sum of the rotationally inelastic cross sections for transitions out of $J=0.5$ F_1 into all higher values of J for both spin–orbit manifolds is identical to that predicted by our present CC calculations, based on the CEPA PES's. In the middle panel, the $F_1 \rightarrow F_1$ CEPA cross sections are compared with those calculated from the earlier electron-gas potential of NPP, as well as from the modified NPP potential used by JAS.[12]

For the fine-structure conserving transitions ($F_1 \rightarrow F_1$), especially for the larger cross sections for low ΔJ, the CEPA cross sections agree well with both experiment and the predictions of the NPP potential. In particular, the residual alternation in the dependence of the cross sections on the final state rotational quantum number, which reveals a small tendency for transitions with even values of ΔJ, is equally apparent in both sets of theoretical cross sections and the set of experimental cross sections. The similarity between the NPP and CEPA cross sections is perhaps surprising, in view of the large difference in the *sum* PES as predicted by the CEPA and electron-gas calculations (see Fig. 4). The modified NPP potential, advocated by JAS,[12] in fact gives poorer agreement with the cross sections based on the *ab initio* CEPA potential. In particular, the modified NPP potential grossly overestimates the cross section for the $J=0.5 \rightarrow 1.5$ transition.

More difference is seen in the lower panel of Fig. 8, which compares the cross sections for spin–orbit changing ($F_1 \rightarrow F_2$) transitions. As previously manifested in the coupled-states[6,53,54] calculations of JAS,[12] the cross sections based on the NPP PES's underestimate by about a factor of 4 the probability of spin–orbit changing transitions. The agreement of the calculations based on the CEPA PES's is considerably better, although the magnitude of the cross sections is still underestimated substan-

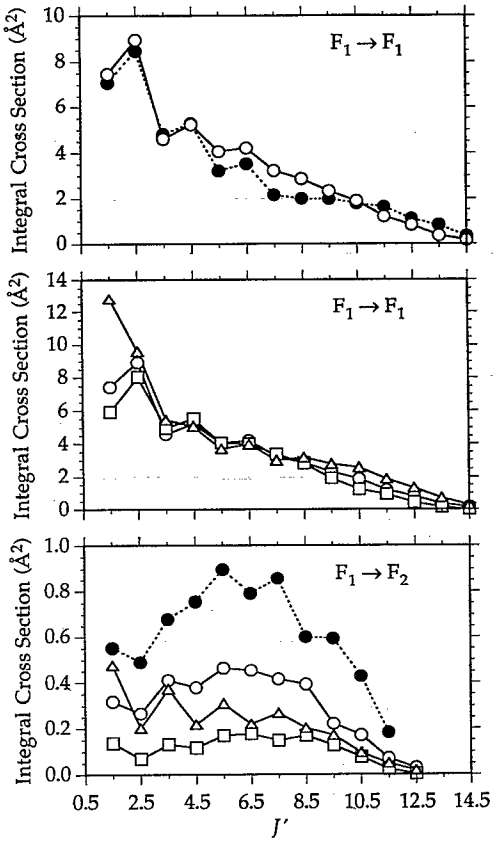

FIG. 8. Close-coupled integral cross sections for the scattering of NO out of the $J=0.5$ level of the lower (F_1) spin–orbit manifold as a function of the final rotational quantum number for transitions into levels of the F_1 and F_2 spin–orbit manifold. The cross sections have been summed over the two Λ-doublet (e/f) levels of the final state and averaged over the two Λ-doublet levels of the initial state [see Eq. (11)]. The initial collision energy is 442 cm^{-1}. The open circles, squares, and triangles refer, respectively, to calculations based on the present CEPA potentials, the earlier NPP electron-gas potentials (Ref. 3), and the modification of the NPP potentials suggested by JAS (Ref. 12). The filled circles represent the experimental values of JAS (Ref. 12), multiplied by a factor of 0.5342, chosen so that the experimental and CEPA total inelastic cross sections, summed over all final states, are identical. For clarity, the comparison of the CEPA cross sections for the $F_1 \rightarrow F_1$ transitions are compared, separately, in the upper panel with experiment, and in the middle panel, with the theoretical cross sections predicted by the NPP and modified NPP potentials.

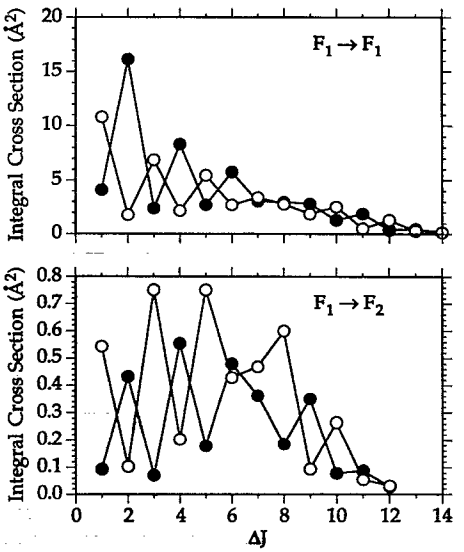

FIG. 9. Close-coupled integral cross sections, determined with the CEPA PES's, for the scattering of NO out of the $J=0.5$ level of the lower (F_1) spin–orbit manifold as a function of the change in rotational quantum number (ΔJ). The filled and open circles designate, respectively, the sum of the cross sections for the two transitions which conserve the parity index ($e \rightarrow e$ and $f \rightarrow f$) and for the two transitions which change the parity index ($e \rightarrow f$ and $f \rightarrow e$) [see Eq. (12)].

tially. The modified NPP potential of JAS[12] predicts larger $F_1 \rightarrow F_2$ cross sections, but overexaggerates, compared both to experiment and the CEPA cross sections, the alternation of the cross sections with final state rotational quantum number.

These alternations have been attributed[11,12] to the near-homonuclear character of the electronic charge distribution of NO, with the result that the *even-*λ terms in the expansion of both the sum and difference PES's will dominate, at least for smaller values of λ. As discussed in the preceding section, these *even-*λ terms will couple the e/f conserving transitions for *odd* ΔJ and the e/f changing transitions for *even* ΔJ. To investigate in more detail the effect of this near-homonuclear character, it is useful to define e/f conserving and e/f changing cross sections as follows:

$$\sigma(JF_1 \rightarrow J'F_1; \epsilon = \epsilon') = \sigma(JF_1 e \rightarrow J'F_1 e) + \sigma(JF_1 f \rightarrow J'F_1 f), \quad (12a)$$

$$\sigma(JF_1 \rightarrow J'F_1; \epsilon \neq \epsilon') = \sigma(JF_1 e \rightarrow J'F_1 f) + \sigma(JF_1 f \rightarrow J'F_1 e). \quad (12b)$$

These e/f conserving and changing cross sections are displayed in Fig. 9 and show clearly the predicted alternation for both the $F_1 \rightarrow F_1$ and $F_1 \rightarrow F_2$ transitions. Since the Λ-doublet averaged cross sections [Eq. (11)] represent the sums of these e/f conserving and changing cross sections, the alternation pattern, seen so dramatically in Fig. 9, is considerably effaced in Fig. 8.

As also discussed in the preceding section, for transitions out of a low-J level, well-described in Hund's case (a), into a higher level, which is no longer well described in case (a), there should appear a propensity for population of Λ-doublet levels of a particular reflection symmetry with respect to the plane of rotation of the molecule. Since this propensity will be independent of the parity index of the initial state, it should be apparent even for scattering out of a rotational level with equal population in both Λ-doublet levels. To investigate this effect, we plot in Fig. 10 the cross sections for population of the Λ-doublet levels of A' and A'' reflection symmetry defined in Eq. (10).

For the fine-structure conserving cross sections, we see, as anticipated earlier, that for low values of the final rotational quantum number, there is no preference for population of states of either A' or A'' reflection symmetry. As J'

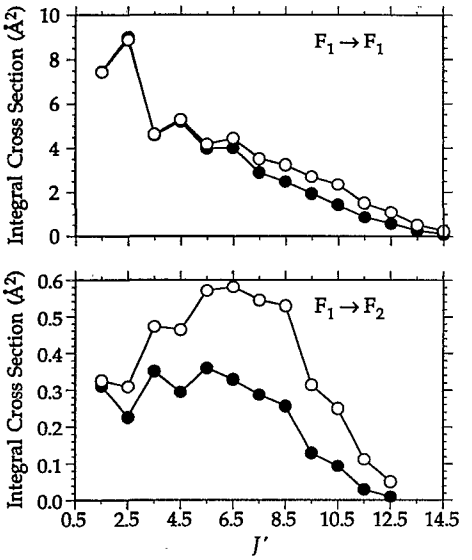

FIG. 10. Close-coupled integral cross sections, determined with the CEPA PES's, for the scattering of NO out of the $J=0.5$ level of the lower (F_1) spin–orbit manifold as a function of the rotational quantum number of the final state. The filled and open circles designate, respectively, the sum of the cross sections for the two transitions which populate rotation levels of nominal A' reflection symmetry and for the two transitions which populate level of nominal A'' reflection symmetry [see Eq. (10)].

increases, we do observe a slight, but noticeable tendency to populate preferentially states of A'' reflection symmetry. A more dramatic propensity, but still favoring states of A'' reflection symmetry, is seen in the cross sections for spin–orbit changing transitions, shown in the lower panel of Fig. 10.

The lower panel of Fig. 10 has important implications for the comparison between calculated and experimentally derived integral cross sections for the spin–orbit changing transitions, particularly when laser induced fluorescence on the NO A–X band system is used to determine the final state distributions. Since noticeably larger cross sections are predicted for transitions into levels of A'' reflection symmetry, the experimentally derived magnitude of the cross sections will depend crucially on whether the populations of the inelastically scattered molecules are probed via main branch P_{ii} or R_{ii} lines (and Q_{ij} satellite branch lines), which will excite out of X state levels of A' reflection symmetry,[48] or main branch Q_{ii} lines (and P_{ij} or R_{ij} satellite branch lines), which will excite out of levels of A'' reflection symmetry. Unfortunately, this information was not reported by JAS.[11,12,55]

In an earlier discussion of collisions involving molecules in $^2\Pi$ molecules which could be described in intermediate case coupling, or, eventually, in the pure Hund's case (b) limit, Dagdigian, Alexander, and Liu[8] proposed a formal propensity rule which stated that if, for perpendicular approach of the atom, the $V_{A'}$ potential were *more repulsive* than the $V_{A''}$ potential, then transitions into levels of A'' reflection symmetry would be favored, regardless of the initial Λ-doublet level considered. This prediction was based on examination of the relative size of the coupling matrix elements between particular pairs of initial and final states. As discussed earlier, this argument cannot be used in the present case, because for NO, sizable mixing of the $\Omega=1/2$ and $\Omega=3/2$ wave functions only occurs for $J>10.5$. However, there is no direct coupling between the $J=0.5$ state and final states with $J>10.5$. Nevertheless, the prediction of a propensity for population of the levels of A'' symmetry does appear to be clearly apparent in our calculated cross sections.

VI. DIFFERENTIAL INELASTIC CROSS SECTIONS

A first comparison is devoted to the dependence on the final-state rotational quantum number of the differential cross sections for transitions out of the $J=0.5$ F_1 level for a constant center-of-mass scattering angle θ. The upper and lower panels of Fig. 11 present differential cross sections for, respectively, fine-structure-conserving ($F_1 \rightarrow F_1$) and fine-structure-changing ($F_1 \rightarrow F_2$) transitions at $E=442$ cm^{-1}. To simulate the averaging over center-of-mass angles resulting from the finite angular acceptance in the experiment, before comparison with experiment the theoretical differential cross sections were convoluted with a detector function

$$d\sigma(JF_i \rightarrow J'F_i')/d\theta = \int d\sigma(JF_i \rightarrow J'F_i')/d\theta' f(\theta') d\theta'. \tag{13}$$

Most appropriate to the experiments of Jons *et al.* is a step function[56]

$$f(\theta)=1/\delta, \quad \theta_0-\delta/2 \leqslant \theta \leqslant \theta_0-\delta/2, \tag{14a}$$

$$f(\theta)=0, \quad \text{otherwise} \tag{14b}$$

spanning an angular range of $\delta=9°$ about the nominal center-of-mass angle.

We observe in the upper panel of Fig. 11 an excellent qualitative agreement between the experimental differential cross sections and the calculated quantities based on the present CEPA PES's. The published values of the experimental cross sections, which are only relative quantities, have been multiplied by a factor of 0.454, chosen so that the sum of the rotationally inelastic differential cross sections at a nominal angle of 50° for transitions out of $J=0.5$ F_1 into all higher values of J for both spin–orbit manifolds, is identical to that predicted by our present CC calculations based on the CEPA PES's. The similarity between this factor and that used in the preceding section to normalize the experimental *integral* cross sections (0.534) is purely coincidental.

For the fine-structure conserving transitions, we observe excellent qualitative agreement between experiment and the theoretical calculations based on the CEPA PES's, in particular, the location of the double rotational rainbow[57,58] with peaks at $J'=2.5$–3.5 and 6.5–8.5. Although the differences between the calculated and theoretical values are somewhat larger than the experimental error bars, the overall agreement is much better than with the differential cross sections calculated from the NPP potential. This difference should be contrasted with the relatively

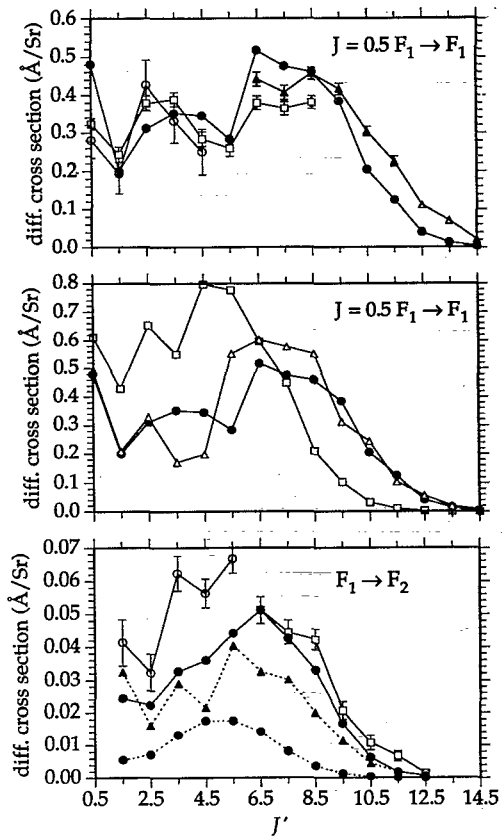

FIG. 11. A comparison of experimental and theoretical differential cross sections for the scattering of NO (J=0.5, F_1) by Ar at an initial collision energy of 442 cm^{-1} and a nominal center-of-mass angle of 50°. The upper two panels display cross sections for fine-structure conserving transitions ($F_1 \rightarrow F_1$), while the lower panel displays cross sections for spin–orbit changing transitions ($F_1 \rightarrow F_2$). As discussed in the text, all the experimental values (and associated error bars) from Refs. 19 and 20 have been multiplied by the factor of 0.454. In all panels, the filled circles connected by solid curves refer to fine-structure averaged cross sections resulting from our close-coupled calculations based on the CEPA PES's. In the upper panel, the open circles, open squares, and open triangles refer to the experimental cross sections determined by LIF detection by means of, respectively, the $R_{11}+Q_{21}$, R_{21}, and $Q_{11}+P_{21}$ branches of the A–X band system. In the middle panel, the open squares and open triangles designate, respectively, cross sections calculated using the original NPP PES's of Ref. 3. and the modified NPP PES's of Ref. 12. In the lower panel, the open circles and open squares refer, respectively, to experimental cross sections into NO levels probed by the $Q_{22}+R_{12}$ and $P_{22}+Q_{12}$ branches of the A–X band system. In addition, in the lower panel, the filled circles and filled triangles, connected by *dashed* lines, designate, respectively, cross sections calculated using the original NPP PES's of Ref. 3 and the modified NPP PES's of Ref. 12.

good agreement between the CEPA and NPP predictions of the integral cross sections, seen in Fig. 7. This confirms the commonly held prejudice that differential inelastic cross sections provide more detailed and subtle information on the fine details of molecular interaction potentials than do integral inelastic cross sections.

For the spin–orbit changing transitions (the lower panel of Fig. 11), we also observe an excellent degree of experiment between the experimentally derived differential cross sections and the close-coupled predictions using our CEPA PES's. The reader should remember that the experimentally derived spin-changing cross sections have *not* been separately normalized. In particular, we observe that the CEPA PES's do not appear to underestimate the $F_1 \rightarrow F_2$ differential cross sections as significantly as in the case of the integral cross sections (see Fig. 8).

We observe in Fig. 11 that in the case of the spin–orbit conserving transitions, the cross sections predicted by the original electron gas PES's of NPP show considerable qualitative differences with both experiment and the CEPA predictions, and in the case of the spin–orbit changing transitions, are noticeably too small. For the spin–orbit conserving transitions, the modified NPP PES's of Ref. 12 show somewhat better agreement, but, however, do not describe well the first rotational rainbow at $J' \sim 3.5$. The cross sections for the spin–orbit-changing transitions are predicted better by the modified[12] NPP PES's. Indeed, for the $F_1 \rightarrow F_2$ transitions with low ΔJ, the modified[12] NPP cross sections show an alternation which more closely mimics the experimental results than do the CEPA cross sections.

From the discussion at the end of Sec. V, we remember that main branch NO $A \leftarrow X$ Q lines will probe rotational levels of nominal $\Pi(A'')$ reflection symmetry, while the main branch P or R lines will probe levels of $\Pi(A')$ reflection symmetry.[48] Thus, the experimental points shown in Fig. 11 reveal a definite tendency (except for the $F_1 \rightarrow F_1$ transitions with low ΔJ) toward population of $\Pi(A'')$ levels. This observation is entirely consistent with the propensity found in our close-coupling calculations using the CEPA PES's, as is shown by Fig. 12. This latter figure compares the definite symmetry *differential* inelastic cross sections, defined analogously to Eq. (11), with the experimental results. As discussed at the end of the preceding section, this propensity toward population of the $\Pi(A'')$ levels is also consistent with the earlier prediction of Daggidian and co-workers[8] based on consideration of the relative degree of repulsivity of the $V_{A'}$ and $V_{A''}$ potential energy surfaces.

Jons *et al.*[20] reported differential cross sections for $F_1 \rightarrow F_1$ transitions at a nominal center-of-mass angle of 95° and two lower center-of-mass energies (149 and 119 cm^{-1}). The upper and lower panels of Fig. 13 present the differential cross sections at a nominal center-of-mass angle of 95° for $F_1 \rightarrow F_1$ transitions at these two energies. In both cases, P_{11} lines were used in the detection, so that the experiment monitors transitions into levels of $\Pi(A')$ reflection symmetry.[48] Fine-structure changing ($F_1 \rightarrow F_2$) transitions are not possible at E=119 cm^{-1} since the upper spin–orbit manifold is energetically closed at this energy. Experimental values of the differential cross sections for these $F_1 \rightarrow F_2$ E=149 cm^{-1} were not reported; presumably they will be very small, since the upper spin–orbit manifold will be barely open.

As in the case of the comparison at 442 cm^{-1}, the agreement between theory and experiment is quite satisfactory at these lower energies, although the position of the first rainbow maxima appears shifted up by one rotational level in the theoretical calculations, similar to what was found at the higher energy (see Fig. 11). The theoretical

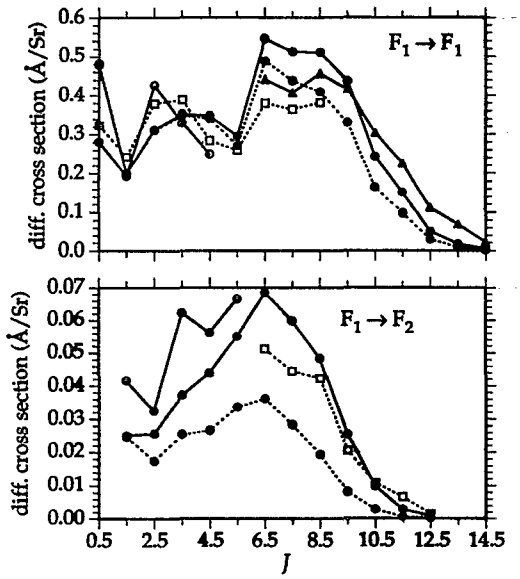

FIG. 12. A comparison of experimental and theoretical differential cross sections for the scattering of NO (J=0.5, F_1) by Ar at an initial collision energy of 442 cm^{-1} and a nominal center-of-mass angle of 50°. The upper panel displays cross sections for fine-structure conserving transitions ($F_1 \rightarrow F_1$) and the lower panel displays cross sections for spin–orbit changing transitions ($F_1 \rightarrow F_2$). As discussed in the text, all the experimental values of Refs. 19 and 20 have been multiplied by a factor of 0.454. The open circles, open squares, and open triangles refer to the experimental cross sections determined by LIF detection by means of, respectively, the $R_{11}+Q_{21}$, R_{21}, and $Q_{11}+P_{21}$ branches of the A–X band system. The filled circles refer to definite-symmetry cross sections [Eq. (10)] resulting from our close-coupled calculations based on the CEPA PES's described here. For both the experimental and theoretical points, the solid curves indicate transitions into levels in which the electronic wave functions are of nominal $\Pi(A'')$ reflection symmetry (Ref. 48), and the dashed curves indicate transitions into levels in which the electronic wave functions are of nominal $\Pi(A')$ reflection symmetry.

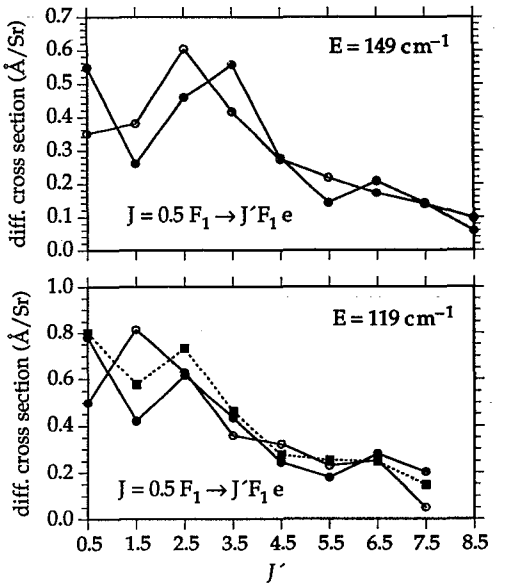

FIG. 13. A comparison of experimental (open circles) and theoretical (filled circles) differential cross sections for the scattering of NO (J=0.5, $F_1 \rightarrow J' F_1 e$) by Ar at initial collision energies of 147 (upper panel) and 119 cm^{-1} (lower panel) and a nominal center-of-mass angle of 95°. The experimental values (and associated error values) of Ref. 20 have been multiplied by factors of 0.22 (upper panel) and 0.323 (lower panel) chosen so that the sums of the displayed differential cross sections are identical. In all cases, the theoretical definite-symmetry, differential cross sections [see Eq. (10)] have been averaged over a 9° wide step detector function. In the lower panel, the filled squares, connected by a dashed line, denote theoretical cross sections which have been additionally averaged [Eq. (15)] over a Gaussian distribution of initial translational energies with a full width at half-maximum (FWHM) of 25 cm^{-1}.

calculations show a smaller, but obvious, additional maxima at higher J (J=6.5), which is seen in the experimental data at 119, but not at 149 cm^{-1}.

Hitherto, we have compared cross sections calculated at a *single* collision energy with experimental results which represent an average of a small, but perhaps not insignificant, spread in collision energies. To assess the effect of the energy averaging inherent in such a measurement, we have carried out an additional comparison with the experimental measurements at E=119 cm^{-1} and θ=95°. We have calculated angle-averaged [Eq. (13)] differential cross sections at a grid of energies centered at 119 cm^{-1} and then simulated the experimental cross sections by an additional convolution with a Gaussian distribution of initial relative translational energies, namely,

$$d\sigma(JF_i \rightarrow J'F_i')/d\theta = \int d\sigma(JF_i \rightarrow J'F_i', E)/d\theta \, f(E-E_0)dE, \qquad (15)$$

where $f(E-E_0)=N\exp\{-\alpha[(E-E_0)/E_0]^2\}$. Here E_0 is the nominal collision energy (119 cm^{-1}), N is a normalization constant, and the constant α is chosen so that the distribution of translational energies has a full width at half-maximum of 25 cm^{-1}.[56]

The comparison of these energy averaged cross sections with the monoenergetic values appears in the lower panel of Fig. 13. As one might have anticipated, the averaging over translational energies smooths out the structure in the dependence of the cross sections on the final state rotational quantum number. In particular, the modulation depth of the secondary maximum at J'=6.5 is diminished, consistent with experiment. However, despite the energy averaging, experiment and theory remain in disagreement regarding the relative magnitudes of the large cross sections into the J'=1.5 and 2.5 levels.

Finally, Figs. 14 and 15 compare the calculated and experimentally determined dependence on the center-of-mass angle for the differential cross sections for transitions into the J=1.5e, 2.5e, 8.5f, 12.5f, and 14.5f Λ-doublet levels of the F_1 spin–orbit manifolds. Here the initial collision energy was 442 cm^{-1}. As in the previous comparisons, the theoretical differential cross sections were averaged over a 9° wide step detector function. The agreement is qualitatively good, particularly for the transitions with higher ΔJ. The rotational rainbow maxima increases from θ=45° to 105° to 170° as ΔJ increases from 8 to 12 to 14. However, for the transitions with ΔJ=1 and 2, the theoretical calculations show evidence for a relatively long

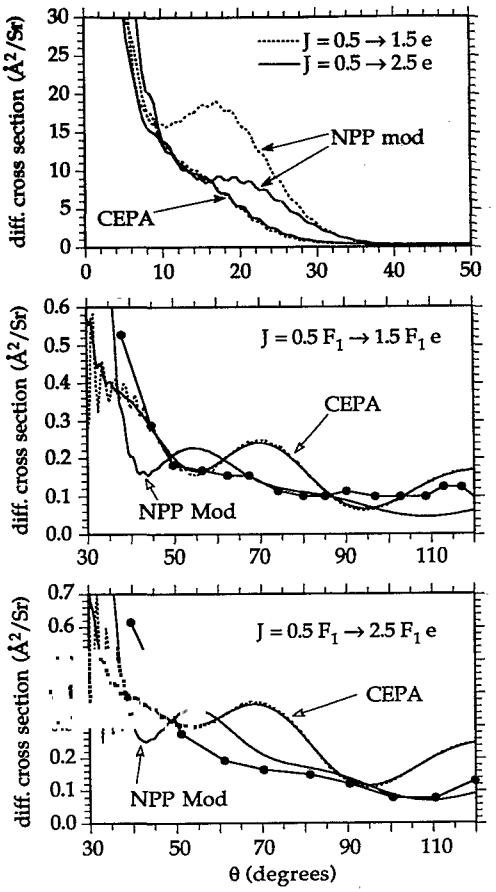

FIG. 14. Differential cross sections for fine-structure conserving $J=0.5$ $F_1 \rightarrow J' F_1 e$ transitions as a function of the center-of-mass angle for the scattering of NO by Ar at an initial collision energy of 442 cm^{-1}. (Upper panel) A comparison of cross sections into the $J'=1.5$ and 2.5 levels from calculations based on the CEPA (solid curves) and the modified NPP (dashed curves) (Ref. 12) PES's. The structure in the cross sections at $\theta=10°$–$20°$ is the rainbow interference pattern due to interference between the inner and outer attractive branches of the attractive potential [experimental (open circles)] and [theoretical (solid curves) (CEPA PES)] differential cross sections as a function of the center-of-mass angle. The calculated differential cross sections have been averaged over a 9° wide step detector function. (Lower two panels) A comparison with experiment. The experimental values from Ref. 20 have been multiplied by, respectively, factors of 0.126 and 0.27, chosen so that to minimize the rms deviation between the CEPA and experimental cross sections at the angles at which measurements were made. In all cases, the theoretical definite-symmetry, differential cross sections [see Eq. (10)] have been averaged over a 9° wide step detector function. The dashed curves indicate the CEPA differential cross sections *before* averaging over this acceptance function.

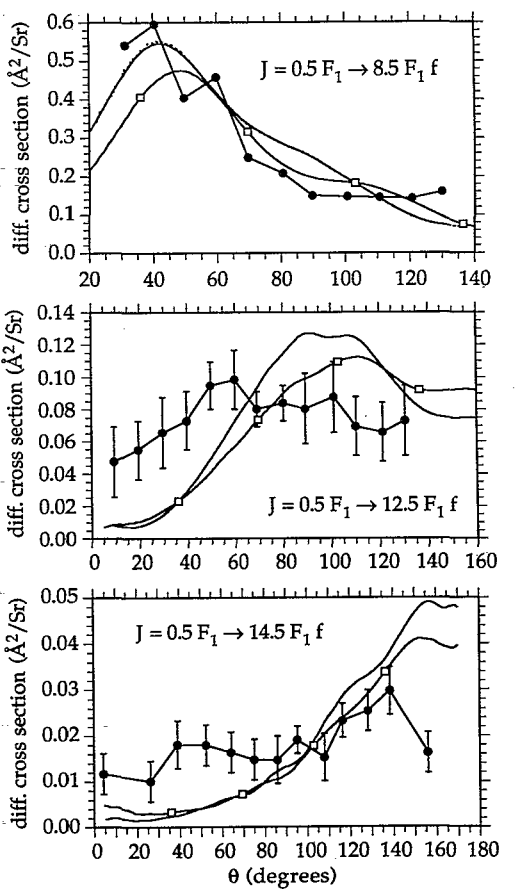

FIG. 15. A comparison of experimental (open circles) and theoretical [(solid curves) CEPA PES's] [(solid curves with open squares) modified NPP PES's] differential cross sections as a function of the center-of-mass angle for the scattering of NO ($J=0.5$, F_1) by Ar at an initial collision energy of 442 cm^{-1}. The three panels display cross sections for fine-structure conserving transitions $J=0.5$ $F_1 \rightarrow J' F_1 f$ with $J'=8.5$, 12.5, and 14.5. The experimental values (and associated error bars) from Ref. 20 have been multiplied by, respectively, factors of 0.37, 0.35, and 0.37, chosen so that to minimize the rms deviation between theory and experiment at the angles at which measurements were made. In all cases, the theoretical definite-symmetry, differential cross sections [see Eq. (10)] have been averaged over a 9° wide step detector function. In the upper panel, the dashed curves indicate the theoretical differential cross sections *before* averaging over this acceptance function.

wavelength oscillation in the differential cross sections. Similar oscillations might be present in the experimental data, although the modulation depth of the oscillations is comparable to the reproducibility error.

These oscillations can likely *not* be attributed to the usual rainbow oscillations due to interference between the inner and outer attractive branches of the attractive potential. As can be seen in the upper panel of Fig. 14, the effect of the attractive rainbow appears at considerably smaller angles. Somewhat similar, as yet unexplained, oscillations have been seen in the rotationally resolved inelastic differential cross sections for the scattering of HF by Ar, reported recently by Rawluk and co-workers.[59] The disappearance of these oscillations in quasiclassical trajectory simulation studies was a clear indication of an origin in quantum interference effects. Recent semiclassical studies indicate that these oscillations reflect interference between the attractive and repulsive branches of the spherically symmetric component of the HF–Ar potential energy surface.[60]

Since the attractive well in the modified NPP potential is deeper than predicted by the present CEPA calculations, and the corresponding attractive rainbow structure is more pronounced (upper panel of Fig. 14), the fall off of the small angle peak occurs at larger angle in the former case. Thus, for the $J=0.5 \rightarrow 1.5$ and 2.5 transitions, the agreement of the angle dependence of the cross sections with experiment is somewhat better for the modified NPP po-

tential. Clearly, though, better discrimination between the various PES's could be achieved if experimental data were available at smaller angles, which would probe the attractive rainbow region.

For the transitions with higher ΔJ, the agreement between the two sets of theoretical differential cross sections (CEPA and modified NPP) is very good. *Qualitatively*, both agree with experiment in that the maxima are shifted towards larger angles with increasing ΔJ. These maxima are certainly the typical rotational rainbow maxima[57,58] seen in prior rotationally resolved studies of deep inelastic scattering governed by repulsive potential energy surfaces. Despite the qualitative agreement with experiment, considerable differences persist. In particular, the theoretical calculations indicate a greater modulation depth in the differential cross sections over the range of angles sampled in the experiment.

VII. DISCUSSION

We have presented here a comparison of differential and integral rotationally resolved cross sections for the inelastic scattering of NO in its electronic ground state ($X\,^2\Pi$) by Ar. *Ab initio* calculations within the correlated electron pair approximation (CEPA) were carried out to obtain a new description of the *two* necessary (A' and A'') Ar–NO potential energy surfaces to supplement the previously available potential energy surfaces based on electron-gas methods. Although good agreement between experiment and theory was achieved, particularly with the new CEPA PES's, considerable differences do persist. In the remainder of this section, we shall explore some possible origins of these differences.

The new CEPA PES's represent a much more sophisticated description of the Ar–NO interaction than the earlier electron gas PES's. The comparison with configuration interaction calculations, including single and double excitations out of a multiconfiguration SCF wave function, presented in Sec. II, confirmed the overall quality of the CEPA calculations, which are less computationally demanding. In addition, our investigation revealed that the calculated interaction potentials would be rendered only slightly less repulsive by the use of a larger atomic orbital basis set including g functions on each of the atoms. Accordingly, and since the present calculations did not explicitly include triple (and higher order) excitations out of the MCSCF wave function, we anticipate that the depth of the attractive well may well be as much as 20% deeper than our predictions. This might engender errors in the description of the shape of the repulsive part of the potential as it rises out of the well. Notwithstanding, we believe that the overall features of the calculated differential cross sections will be little altered, especially at the higher energy (442 cm^{-1}) considered in the experiments of Jons *et al.*[19,20] and for center-of-mass angles that lead to substantial inelasticity.

The molecular-beam, electric-resonance experiments of Howard and co-workers[13,14] provide additional information on the Ar–NO PES's in the region of the van der Waals minimum. A preliminary investigation[61] indicates good agreement between the experimental spectra and theoretical predictions based on the CEPA PES's, but considerable disagreement with predictions based on each of the other (NPP,[3] modified NPP,[12] and empirical[10]) potentials considered here.

Although a complete close coupling description was used in the scattering calculations, we assumed that the approach of the Ar atom led to no change in the magnitude of the NO spin–orbit constant, which is responsible for the splitting between the F_1 and F_2 manifolds. This change will likely be relatively small in the present case since the weak bonding in the Ar–NO van der Waals complex is not likely to induce a sizable change in the NO electronic wave function. This assumption is supported by the recent work of Lester and collaborators on the Ar–OH($X\,^2\Pi$) van der Waals molecule, where the splitting between the two spin–orbit manifolds was found to be within 10% of the splitting in the isolated OH radical.[62]

An additional source of error could arise from the comparison of theoretical differential or integral cross sections, determined at a particular collision energy E, with experimental cross sections which represent an average over a distribution of energies centered about E. An investigation of the effect of energy averaging requires a number of additional scattering calculations at energies which span the experimental distribution in translational energies. Because of the larger computer time requirement for the scattering calculations at the higher energies considered (particularly 442 cm^{-1}), we investigated the effect of energy averaging only at the lowest energy studied experimentally (119 cm^{-1}). At this energy, only relatively small changes were found in the predicted cross sections. Nonetheless, future work should be directed toward an exploration of the effect of energy averaging at the higher nominal translational energies.

An additional source of discrepancy between the calculated and experimental cross sections would be due to rotational polarization of the scattered molecules. The calculated differential cross sections represent the sum over all accessible final m_J states. Although all m_J states are equally populated in the incoming NO beam, a collision with Ar might result in a preferential population of certain final m_J states. Under beam conditions, any spectroscopic detection technique will be preferentially sensitive to a certain subset of m_J states (depending on which spectral line is used). It could be this effect, rather than the preferential population of the A'' Λ-doublet levels, which is responsible for the observed difference (see Fig. 11) in the differential cross sections as measured by the main-branch Q, as compared to P or R, lines. Additional theoretical calculations should investigate whether one might expect a significant degree of rotational polarization of the scattered molecules.

Along with the further theoretical studies, suggested above, we encourage additional investigations by our experimental colleagues. In particular, the upper panel of Fig. 14 suggests that an investigation of the angle dependence of the differential cross sections for small scattering angle and for small ΔJ, albeit perhaps technically difficult, would certainly help to discriminate among the theoretical

potential energy surfaces. Similarly, a further characterization of the full energy dependence of differential cross sections for one (or several) angles and for one (or several) transitions would provide a valuable calibration of the theory. Additionally, the determination of *absolute* differential cross section, even at just one scattering angle, would provide an additional, stringent test of the theoretical potential energy surfaces and scattering calculations.

ACKNOWLEDGMENTS

The author wishes to thank the National Science Foundation for support of the research reported here under Grant No. CHE-923081. He is grateful to Ron Gentry, Ben Whitaker, and Paul Houston for their encouragement, as well as stimulating discussions and additional information about the experiments reported in Refs. 19–22, to John Ashenfelter for his help with the *ab initio* calculations reported in Sec. II, and to Hans-Joachim Werner for valuable discussions of the results of these calculations.

[1] K. Bergmann and W. Demtröder, Z. Phys. **243**, 1 (1971).
[2] H. Klar, J. Phys. B **6**, 2139 (1973).
[3] G. C. Nielson, G. A. Parker, and R. T Pack, J. Chem. Phys. **66**, 1396 (1977).
[4] S. Green and R. N. Zare, Chem. Phys. **7**, 62 (1975).
[5] M. H. Alexander, J. Chem. Phys. **76**, 5974 (1982).
[6] M. H. Alexander, Chem. Phys. **92**, 337 (1985).
[7] M. H. Alexander and B. Pouilly, J. Chem. Phys. **79**, 1545 (1983).
[8] P. J. Dagdigian, M. H. Alexander, and K. Liu, J. Chem. Phys. **91**, 839 (1989).
[9] H. H. W. Thuis, S. Stolte, J. Reuss, J. J. H. van der Biesen, and C. C. H. van der Meijdenberg, Chem. Phys. **52**, 211 (1980).
[10] P. Casavecchia, A. Laganà, and G. G. Volpi, Chem. Phys. Lett. **112**, 445 (1984).
[11] P. Andresen, H. Joswig, H. Pauly, and R. Schinke, J. Chem. Phys. **77**, 2204 (1982).
[12] H. Joswig, P. Andresen, and R. Schinke, J. Chem. Phys. **85**, 1904 (1986).
[13] B. J. Howard, C. M. Western, and P. D. Mills, Faraday Discuss. Chem. Soc. **73**, 129 (1982).
[14] C. M. Western and B. J. Howard, J. Phys. Chem. **90**, 4961 (1986).
[15] R. G. Gordon and Y. S. Kim, J. Chem. Phys. **56**, 3122 (1972); Y. S. Kim and R. G. Gordon, *ibid.* **60**, 1842 (1974).
[16] T. Orlikowski and M. H. Alexander, J. Chem. Phys. **79**, 6006 (1983).
[17] M. H. Alexander and T. Orlikowski, J. Chem. Phys. **80**, 1506 (1984).
[18] T. Orlikowski and M. H. Alexander, J. Chem. Phys. **80**, 4133 (1984).
[19] S. D. Jons, J. E. Shirley, M. T. Vonk, C. F. Giese, and W. R. Gentry, J. Chem. Phys. **97**, 7831 (1992).
[20] S. D. Jons, Ph. D. thesis, University of Minnesota, 1992.
[21] A. G. Suits, L. S. Bontuyan, P. L. Houston, and B. J. Whitaker, J. Chem. Phys. **96**, 8618 (1992).
[22] L. S. Bontuyan, A. G. Suits, P. L. Houston, and B. J. Whitaker, J. Phys. Chem. **97**, 6342 (1993).
[23] W. Meyer, Int. J. Quantum Chem. Symp. **5**, 341 (1971).
[24] W. Meyer, J. Chem. Phys. **58**, 1017 (1973).
[25] W. Meyer, Theoret. Chim. Acta **35**, 277 (1974).
[26] R. Jonas and V. Staemmler, Z. Phys. D **14**, 143 (1989).
[27] A. Jörg, A. Degli-Esposti, and H.-J. Werner, J. Chem. Phys. **93**, 8757 (1990).
[28] A. Degli-Esposti and H.-J. Werner, J. Chem. Phys. **93**, 3351 (1990).
[29] T. H. Dunning, Jr., J. Chem. Phys. **90**, 1007 (1989).
[30] R. A. Kendall, T. H. Dunning, Jr., and R. J. Harrison, J. Chem. Phys. **96**, 6796 (1992).
[31] K. P. Huber and G. Herzberg, *Molecular Spectra and Molecular Structure. IV. Constants of Diatomic Molecules* (Van Nostrand–Reinhold, New York, 1979).
[32] MOLPRO is a package of *ab initio* programs written by H.-J. Werner and P. J. Knowles with contributions from J. Almlöf, R. Amos, S. Elbert, W. Meyer, E. A. Reinsch, R. Pitzer, and A. Stone.
[33] S. F. Boys and F. Benardi, Mol. Phys. **19**, 553 (1970).
[34] H.-J. Werner and E. A. Reinsch, J. Chem. Phys. **76**, 3144 (1982).
[35] H.-J. Werner and E. A. Reinsch, in *Advanced Theories and Computational Approaches to the Electronic Structure of Molecules*, edited by C. E. Dykstra (Reidel, Dordrecht, 1984), p. 79.
[36] R. J. Gadnitz and R. Alrichs, Chem. Phys. Lett. **143**, 413 (1988).
[37] Tables of the expansion coefficients in Eq. (3), as well as a FORTRAN program to determine the radial expansion coefficients $V_\lambda(R)$ in the expansion of $V_{\rm sum}$ and $V_{\rm dif}$ as a function of R are available on request from the author by electronic mail (address: mha@hibridon.umd.edu). Please supply a return electronic mail address.
[38] D. M. Brink and G. R. Satchler, *Angular Momentum*, 2nd ed. (Clarendon, Oxford, 1968).
[39] R. N. Zare, A. L. Schmeltekopf, W. J. Harrop, and D. L. Albritton, J. Mol. Spectrosc. **46**, 37 (1973).
[40] M. H. Alexander and P. J. Dagdigian, J. Chem. Phys. **80**, 4325 (1984).
[41] J. M. Brown, J. T. Hougen, K.-P. Huber, J. W. C. Johns, I. Kopp, H. Lefebvre-Brion, A. J. Merer, D. A. Ramsay, J. Rostas, and R. N. Zare, J. Mol. Spectrosc. **55**, 500 (1975).
[42] H. Lefebvre-Brion and R. W. Field, *Perturbations in the Spectra of Diatomic Molecules* (Academic, New York, 1986).
[43] J. T. Hougen, Natl. Bur. Stand. (U.S.) Monograph 115, 1970.
[44] J. E. Smedley, G. C. Corey, and M. H. Alexander, J. Chem. Phys. **87**, 3218 (1987).
[45] A. Arthurs and A. Dalgarno, Proc. R. Soc. London Ser. A **256**, 540 (1960).
[46] W. A. Lester, Jr., Meth. Comp. Phys. **10**, 211 (1971).
[47] M. H. Alexander, W. Kearney, and A. F. Wagner, J. Chem. Phys. (to be published).
[48] M. H. Alexander, P. Andresen, R. Bacis, R. Bersohn, F. J. Comes, P. J. Dagdigian, R. N. Dixon, R. W. Field, G. W. Flynn, K.-H. Gericke, B. J. Howard, J. R. Huber, D. S. King, J. L. Kinsey, K. Kleinermanns, A. C. Luntz, A. J. MacCaffery, B. Pouilly, H. Reisler, S. Rosenwaks, E. Rothe, M. Shapiro, J. P. Simons, R. Vasudev, J. R. Wiesenfeld, C. Wittig, and R. N. Zare, J. Chem. Phys. **89**, 1749 (1988).
[49] M. H. Alexander, J. Chem. Phys. **80**, 3485 (1984).
[50] D. Secrest, J. Chem. Phys. **62**, 710 (1975).
[51] D. J. Kouri and R. B. Gerber, Isr. J. Chem. **22**, 321 (1982), and references contained therein.
[52] M. H. Alexander, J. Chem. Phys. **94**, 8468 (1991).
[53] D. J. Kouri, in *Atom–Molecule Collision Theory: A Guide for the Experimentalist*, edited by R. B. Berstein (Plenum, New York, 1979), p. 301.
[54] M. H. Alexander and D. C. Clary, Chem. Phys. Lett. **97**, 319 (1983).
[55] P. Andresen (private communication, 1993).
[56] R. Gentry (private communication, 1993).
[57] R. Schinke and J. M. Bowman, in *Molecular Collision Dynamics*, edited by J. M. Bowman (Springer, Berlin, 1982), Chap. 3.
[58] K. Bergmann, U. Hefter, A. Mattheus, and J. Witt, Chem. Phys. Lett. **78**, 61 (1981).
[59] L. J. Rawluk, M. Keil, M. H. Alexander, H. R. Mayne, and J. J. C. Barrett, Chem. Phys. Lett. **202**, 291 (1992).
[60] J. J. C. Barrett, H. R. Mayne, and M. Keil, J. Chem. Phys. (to be published).
[61] T. Schmelz, P. Rosmus, and M. H. Alexander (to be published).
[62] M. T. Berry, M. R. Brustein, M. I. Lester, C. Chakravarty, and D. C. Clary, Chem. Phys. Lett. **178**, 301 (1991).